



Study of jumping water droplets on superhydrophobic surfaces with electric fields



B. Traipattanakul^a, C.Y. Tso^{a,b}, Christopher Y.H. Chao^{a,*}

^aDepartment of Mechanical and Aerospace Engineering, The Hong Kong University of Science and Technology (HKUST), Clear Water Bay, Kowloon, Hong Kong, China

^bHKUST Jockey Club Institute for Advanced Study, The Hong Kong University of Science and Technology (HKUST), Clear Water Bay, Kowloon, Hong Kong, China

ARTICLE INFO

Article history:

Received 24 March 2017

Received in revised form 20 July 2017

Accepted 20 July 2017

Keywords:

Charge

Droplets

Electric field

Jumping

Superhydrophobic surface

ABSTRACT

Macro-sized droplets adhering to non-wetting surfaces, a phenomenon referred to as progressive flooding, is one of the major problematic issues found on a superhydrophobic condenser, which reduces the heat and mass transfer performance. Utilization of an electric field on superhydrophobic surfaces can potentially address this problem. In this study, a water droplet is placed on a superhydrophobic plate which is in parallel to another plate. A positive electrode and a ground line are connected to the bottom plate and the top plate, respectively. The droplet motion is recorded by a high-speed camera and analyzed in sequential frames. This work aims to investigate the electrical voltage threshold, the electric field threshold and the droplet charge required to remove a macro-sized droplet from a superhydrophobic surface. The results show that with an increase in gap width, both the electrical voltage threshold and the electric field threshold increase, while the droplet charge decreases. Additionally, the results of this study also reveal a constant electrostatic force acting on droplets in the air and the maximum electrostatic force acting on droplets on the superhydrophobic surface regardless of the gap width and of applied electric field intensity. This work can offer a platform for improving the performance of self-cleaning surfaces, thermal diodes/switches and anti-icing surfaces.

© 2017 Elsevier Ltd. All rights reserved.

1. Introduction

Condensation heat transfer processes can be found in thermal management systems [1,2], power generation systems [3] and water harvesting systems [4]. On a non-wetting surface, small spherical condensates, the result of dropwise condensation, have the potential to enhance heat transfer much more than filmwise condensation [5–7]. When droplets coalesce on the surface, excess surface energy converts to kinetic energy leading to a jumping phenomenon of coalescing droplets [8–12]. These departing droplets leave new spaces on the surface which can be exposed to the continuing water droplet condensation process [13,14], enhancing heat transfer by 30% compared to the normal dropwise condensation [15,16]. However, gravitational force and vapor flow around the surface can cause jumping droplets to return to the surface [17]. These returning droplets can either coalesce with other neighboring droplets on the surface and jump again, or adhere to the surface. As time progresses, the size of these adhering droplets

become larger, leading to progressive flooding. As a result, condensation heat transfer will be degraded [18]. Electric fields applied between two parallel plates to remove droplets adhering to the surface is one potential method to solve this problem. A number of studies are carried out to investigate the electrostatic-induced jumping water droplets in both horizontal and vertical directions with various electric fields and gap widths.

In the study by Takeda et al. [19], a DC high voltage power supply connected to the glass-coated superhydrophobic surface was used to create a strong vertical electric field between two parallel plates with a gap width of 10 mm. The results showed that a 2-mm diameter droplet can jump to the top plate when a 9 kV voltage was applied. Roux et al. [20] also investigated saturated NaCl solution droplets and 0.5 M NaCl solution droplets on a non-wetting surface in a light-mineral-oil condenser with applied electric fields. Droplets were placed on the surface with the gap width of 33 mm. Mineral oil has the specific density of 0.84, the relative permittivity (ϵ_r) of 2.11 and the electrical conductivity (σ) of 396×10^{-15} S/m. The electric field thresholds of four different droplet sizes were revealed. The results showed that a saturated NaCl solution droplet with a maximum diameter of 1.5 mm required at least 175 V/mm to depart from the surface, while only 125 V/mm was required to induce the jumping of the less condensed 0.5 M NaCl solution

* Corresponding author at: Department of Mechanical and Aerospace Engineering, Main Academic Building, The Hong Kong University of Science and Technology, Clear Water Bay, Kowloon, Hong Kong, China.

E-mail address: meyhchao@ust.hk (C.Y.H. Chao).

Nomenclature

A	droplet cross-sectional area [m ²]	t	time duration [s]
C_D	drag coefficient [–]	V	electrical voltage [V]
E	electric field [V/m]	V_d	droplet volume [m ³]
F_{AD}	maximum adhesion force [N]	v_d	droplet velocity [m/s]
F_W	gravitational force [N]	We	Weber number [–]
F_D	drag force [N]	ε	medium fluid permittivity [F/m]
F_E	electrostatic force [N]	ε_r	relative permittivity [–]
F_B	buoyancy force [N]	θ	contact angle [°]
$F_{E,S}$	maximum electrostatic force [N]	θ_{cr}	critical contact angle [°]
g	gravitational acceleration [m/s ²]	μ	air viscosity [kg/ms]
L	gap width between two plates [m]	ρ_a	air density [kg/m ³]
Q	droplet average charge [C]	ρ_w	water density [kg/m ³]
Re	Reynolds number [–]	γ	water–air surface tension [N/m]
r_o	droplet radius [m]	σ	medium fluid conductivity [S/m]
r_c	contact radius [m]	τ	relaxation time [s]

droplet. In addition, Khayari et al. [21] studied dynamics of a water droplet in corn oil in a vertical electric field. The density of the corn oil is 916 kg/m³, while the permittivity (ε) and the electrical conductivity (σ) are 26.9×10^{-12} F/m and 19×10^{-12} S/m, respectively. The drop radius was 1.337 mm resting on a steel electrode, and the fixed gap width was 20 mm. Their results showed that the electric field threshold for lifting the droplet was approximately 170 V/mm. Furthermore, Khayari and Perez [22] experimentally and theoretically studied the charge acquired by a spherical ball bouncing on an electrode. Three medium fluids, namely corn oil (relative permittivity (ε_r) = 3.04–3.11, conductivity (σ) = 26.2–60.8 $\times 10^{-12}$ S/m), sunflower oil (relative permittivity (ε_r) = 3.04–3.07, conductivity (σ) = 11.0–14.3 $\times 10^{-12}$ S/m), and isopar (relative permittivity (ε_r) = 2.0, conductivity (σ) = 70–317 $\times 10^{-12}$ S/m) were used. The gap widths were 20 mm and 40 mm. The three types of spherical balls were made from a plastic covered by aluminum sheets with the radius of 4 mm, and made from aluminum sheets with the radii of 3.25 mm and 2.33 mm. The experimental results of the electric field threshold ranged between 346 V/mm and 403 V/mm. Additionally, the electrical voltage threshold ranged between 7.1 kV and 16.1 kV. With the same medium fluid and the same gap width, when the droplet size increased, the voltage threshold and the electric field threshold increased. Moreover, Jung et al. [23] studied small water droplets in silicon oil in a horizontal electric field. While the density of the silicon oil is 957.24 kg/m³, the permittivity (ε) and the electrical conductivity (σ) are 24.35×10^{-12} F/m and 1×10^{-13} S/m, respectively. The radius of the droplets ranged from 0.363 mm to 0.726 mm, and the gap width was 10 mm. The results showed that the electrical charging process depended on the electric field strength and the size of a droplet. However, due to the horizontal electric field and the horizontal motion of the droplet, the electric field threshold was not studied. Jalaal et al. [24] also investigated falling water droplets in transformer oil with an applied horizontal electric field. The density of the transformer oil is 841.9 kg/m³. The relative permittivity (ε_r) and the electrical conductivity (σ) are 2.1 and 3.3×10^{-12} S/m, respectively. The droplet diameters ranged from 0.3 mm to 3.5 mm. They found that a high voltage electrode pulled the droplet (i.e. the droplet gained the positive charge after touching the electrode and jumped away due to the electrophoretic force) as the droplet passed through the electric field. Their results also showed that an applied voltage of 6 kV was required to move droplets of 1 mm and 2 mm in diameter between two electrodes, but an electrical voltage of 7.5 kV was needed for droplets with a diameter of 3 mm.

Although the previous studies demonstrated that the electric field can be used to move droplets in various medium fluids and at different fixed gap widths, there is still a lack of understanding of the effects of the electric field threshold and the droplet charge on droplets resting on the superhydrophobic surface with air as the medium fluid. Therefore, this study aims to investigate the effects of the electrical voltage threshold, the electric field threshold and the droplet charge required to remove a macro-sized droplet on a superhydrophobic surface at varying gap widths when air serves as the medium fluid, an area of research which has never been studied before. Moreover, this study is the first study to reveal the electrostatic forces acting on a droplet both in mid-air and on the electrode before lift-off, leading to new understanding of the droplet dynamics in the electric field. Additionally, the charge relaxation time and the lift-off mechanism are discussed and compared with other previous studies. The results of the current study not only can shed more light on the issue of progressive flooding, but also can provide further research value to the areas of self-cleaning [25], thermal diodes [26,27], anti-icing [28] and condensation heat transfer [29].

2. Review of theoretical work

In this section, previous research on coalescing jumping droplets is chronologically and briefly presented in order to provide insight of some major findings in this field. Then, the fundamental physics of the droplet dynamics in an electric field, namely forces acting on a droplet, the lift-off mechanism and charging relaxation time, from previous similar studies are illustrated for later discussion in the current work.

2.1. Background of the coalescing jumping droplets

A great deal of research has been conducted on the coalescence of droplets and the jumping mechanism over the past five years. The following are findings from some important research in this field, presented chronologically. Boreyko and Chen [8] reported that dropwise condensates can coalesce with each other and self-jump from a non-wetting surface as a result of the conversion of excess surface energy to kinetic energy. The coalescing jumping phenomena of two individual drops was observed and the inertial-capillary velocity of such jumping was developed. A study by Nam et al. [9] also showed that a quick increase in kinetic energy of the merging droplets was caused by low pressure at a

liquid bridge and high pressure at the bottom of the droplets. The changes in kinetic energy, surface energy, potential energy and viscous dissipation energy of the merging droplets as a function of time were highlighted. In addition, Liu et al. [10] conducted a lattice Boltzmann simulation based on the pseudo-potential lattice Boltzmann model. Due to numerical instability related to the high fluid density ratio and the viscosity ratio, the equation of state was modified and the multiphase relaxation time method was used. The results showed that when the droplet radius was smaller than 50 μm , the jumping velocity increased with an increase in the droplet radius. However, the jumping velocity decreased with an increase in the droplet size when the droplet radius was larger than 50 μm . These results were in line with experimental results observed in [8]. Moreover, the results obtained from the qualitative analysis showed that the coalescing jumping mechanism can only occur on a sufficiently-high-contact-angle superhydrophobic surface [10]. Later, Liu et al. [11] ran numerical simulations on the coalescing mechanism. The 3D two-droplet coalescence processes on a flat surface and in the air were illustrated, and the velocity of a coalescing droplet as a function of time and Ohnesorge number was shown. Enright et al. [12] also experimentally and numerically studied the coalescing droplet velocity and the internal flow momentum during such mechanism. The results showed that only 6% of excess surface energy was converted to kinetic energy. These jumping incidents of coalescing droplets can enhance the condensation heat transfer.

2.2. Forces acting on a droplet

Coalescing jumping droplets are forced to return to the lower substrate due to the gravitational force and vapor flow near a superhydrophobic surface. Some of these returning droplets adhere to the surface and continue to grow in size, leading to progressive flooding. To permanently remove macro-sized droplets resting on the superhydrophobic surface, an applied external force is required to overcome the adhesion force on the surface, the gravitational force due to the droplet volume and the mid-flight drag force. In an electric field, this applied external force is solely the electrostatic force. In this section, a review of theoretical work on the electrostatic force along with other forces acting on macro-sized droplets is presented in order to provide basic understanding of the force analysis of the droplet dynamics in the electric field.

Roux et al. [20] explained that the droplet resting on the substrate of the electrode can acquire Maxwell's charge. This charge was categorized as induction charging because the contact potential charging was neglected due to the large particle size (i.e. larger than 1 μm) [30]. The results of the droplet charge in Roux et al.'s study [20] were in line with a modified mathematical model that was originally proposed by Lebedev and Skal'skaya [31]. Khayari et al. [21] also calculated the initial charge of the droplet particle from Maxwell's charge. However, it should be noted that Maxwell's charge is valid if and only if the radius of the particle (r_0) is much less than the gap width between two parallel electrodes (L).

In terms of force analysis, Takeda et al. [19] stated that resistance forces in this experiment consisted of adhesion and gravitational forces. Both depended on the size of the droplet, but the adhesion force relied on the contact line, while the gravitational force varied with the volume of the droplet. In other words, when the droplet size increased, the electric field threshold also increased. Thus, in order to lift up the macro-sized droplets, the electrostatic force must be higher than the sum of the gravitational and adhesion forces. Moreover, Roux et al.'s study [20] described four forces acting on a droplet on a substrate prior to lift-off. The first force is the coulombic force or the electrostatic force. The second one is the gravitational force due to the droplet volume. The third force is the buoyancy force, and the last one is the reaction

force from the substrate. The similar analysis was reported in the study by Khayari et al. [21]. However, the two studies differ in their methods of determining the electric field threshold [20,21]. The electric field threshold in [20] was determined when the droplet started lifting with zero adhesion force, while the threshold in [21] was calculated using all forces including the adhesion force. Moreover, it should be noted that studies [20,21] lacked an analysis of forces acting on the airborne jumping droplets. In the study by Jung et al. [23] where the charging droplet moved horizontally in a horizontal electric field, forces acting on an airborne moving droplet were considered. Only the drag force and the electrostatic force were taken into account. Moreover, creeping flow was assumed and the drag force was determined using the Hadamard-Rybczynski solution. The results showed that the electrical charge of the droplet is directly proportional to the dynamic viscosity of the medium fluid, the droplet velocity and the droplet radius, and is inversely proportional to the applied electric field. This means that when the electric field increases, the droplet charge decreases in the horizontal electric field.

2.3. The lift-off mechanism

Apart from the force analysis, the lift-off mechanism of a droplet on a substrate is also crucial. In Khayari et al.'s study [21], a steel electrode was placed in corn oil. At the beginning, it was observed that, without the electric field, the geometry of the droplet was spherical with a contact angle of 160°. When the electric field threshold of 170 V/mm was applied, the contact angle decreased to 115°. This lift-off mechanism was also studied by Gliere et al. [32]. As the electric field approached the threshold value, the droplet elongated. As a result, the contact angle decreased, leading to an increase in the adhesion force between the droplet and the surface of the electrode. The study [32] also showed that when the receding angle or 90° contact angle was reached due to the applied electric field, the contact line between the interface and the electrode collapsed resulting in the droplet's lift-off, and this amount of the applied electric field was called the electric field threshold. Moreover, determining the electrostatic force and the adhesion force of a droplet at the substrate of the electrode can provide more insight into the lift-off mechanism. To do so, the contact radius of a droplet on the superhydrophobic surface needs to first be determined. As illustrated in Fig. 1a, without an applied electric field, a droplet rests on the superhydropho-

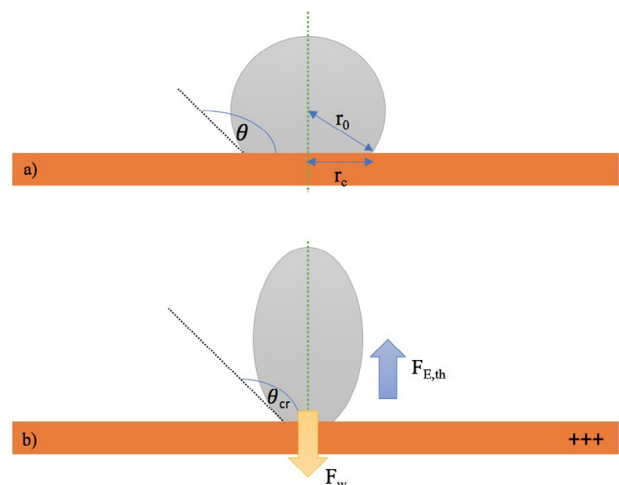


Fig. 1. A schematic diagram of the droplet lift-off mechanism, (a) a droplet on the superhydrophobic surface without an electric field, (b) an elongated droplet before lift-off on the superhydrophobic surface with an electric field.

bic copper plate. The contact radius of the droplet (r_c) can be determined using the trigonometric function of the contact angle (θ) and the droplet radius (r_0) (i.e. $r_c = r_0 \sin \theta$). When an electrical voltage is supplied to the parallel plates, an electric field is created. Fig. 1b shows the elongated droplet when the electric field threshold is reached [32]. The maximum adhesion force can be acquired from Eq. (1).

$$F_{AD} = 2\pi r_c \gamma \sin \theta_{cr}. \quad (1)$$

In this equation, γ and θ_{cr} represent the surface tension of a water droplet and the critical contact angle before lift-off in the electric field, respectively. On the superhydrophobic surface, when an electric field threshold is applied, the maximum adhesion force (F_{AD}), the gravitational force (F_W) and the maximum electrostatic force ($F_{E,S}$) act on the droplet. For the droplet to lift-off, the maximum electrostatic force needs to overcome the summation of the other two forces (i.e. $F_{E,S} = F_{AD} + F_W$). Eq. (1) will be used for analyses and discussions in later sections.

2.4. Charging relaxation time

When a droplet departs from the substrate surface due to the lift-off mechanism mentioned in the previous section, the amount of droplet charge, in some cases, decreases. This is due to the high electrical conductivity of the medium fluid used in a system compared to its own permittivity. In the study by Khayari et al. [21], corn oil which has the electrical conductivity (σ) of 19×10^{-12} S/m and the permittivity (ϵ) of 26.9×10^{-12} F/m was used as the medium fluid. After lift-off, the droplet charge started decaying. This phenomenon is caused by charging relaxation time (τ) which can be determined from the permittivity (ϵ) and the conductivity (σ) of a medium fluid as shown in Eq. (2) [33,34]. This equation will be used in the later sections for analyses and discussions.

$$\tau = \frac{\epsilon}{\sigma}. \quad (2)$$

3. Experimental procedures

3.1. Surface fabrication

Although there are many methods to fabricate superhydrophobic surfaces [35–37], dipping the substrate into chemical substances is one of the most cost-effective and time-efficient methods [38]. In this study, the fabrication method proposed by Larmour et al. [39] is adapted. To fabricate a superhydrophobic surface, 0.01 M of silver nitrate solution (AgNO_3) [40] is used as the nano-coating substance, and 1 mM of heptadecafluoro-1-decathiol $\text{CF}_3(\text{CF}_2)_7\text{CH}_2\text{CH}_2\text{SH}$ called HDFT in dichloromethane (CH_2Cl_2) [41] is used as the water repellent agent.

At the first step of superhydrophobic surface fabrication, the surface of a small copper plate $36 \text{ mm} \times 36 \text{ mm} \times 3.5 \text{ mm}$ is polished using abrasive papers. A 500-grit abrasive paper is applied first followed by 600, 800, 1000, 1200, 1500 and 1600. After applying a 1500-grit sandpaper, the color of the surface should be pinkish gold in color. In this step, all parts of the surface should be polished equally, otherwise, an inclined plane or a bowl shape may occur. After that, the polished copper plate is placed in acetone solution for 10 min to degrease and ethanol solution for another 10 min to remove acetone. The plate is then rinsed with deionized water and dried with nitrogen. It should be noted that the flow rate of the nitrogen stream should be as light as possible for each use in the fabrication procedure. The copper plate is then placed in silver nitrate solution for 10 min. The surface of the copper plate looks very black at this step because nano-textured silver is deposited on the copper plate. The plate is rinsed with deionized

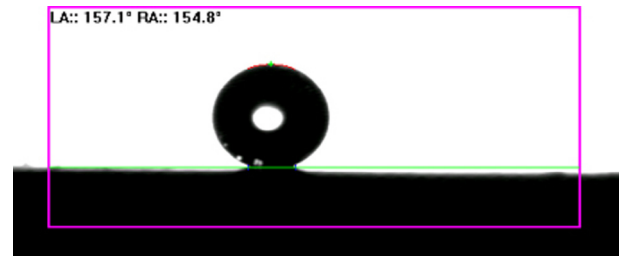


Fig. 2. The static contact angle of a water droplet on the superhydrophobic surface.

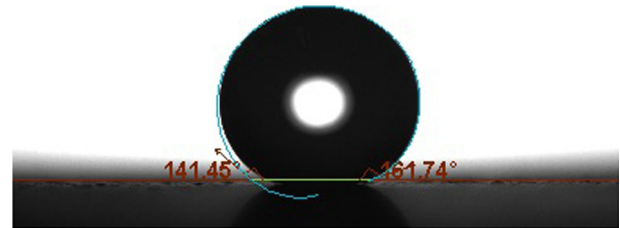


Fig. 3. The dynamic contact angles of a water droplet on the superhydrophobic surface with the advancing contact angle of 161.74° and the receding contact angle of 141.45° .

water and dried with the nitrogen gun. To dehydrate the copper plate, it is again placed in 100 ml of pure ethanol for 1 min. The plate is then gently placed in the HDFT solution for 15 min, then submerged in pure ethanol for 1 min and dried with a nitrogen gun.

The chemical products mentioned are bought from Sigma-Aldrich [38,39]. The contact angle measurement is done with Digidrop Contact Angle meter. The average contact angle of a water droplet is measured at 156° as shown in Fig. 2, implying that the afore-mentioned method for fabricating a superhydrophobic surface is successful. In order to identify the advancing and receding contact angles, the measurement of the dynamic contact angles is also performed. As shown in Fig. 3, the advancing contact angles and the receding contact angles are 161.74° and 141.45° , respectively. Additionally, Fig. 4 shows the surface roughness of the superhydrophobic copper plate. The average surface roughness is approximately $2.15 \mu\text{m}$.

3.2. Experimental setup

Two parallel copper plates are placed with a specified gap. The bottom copper plate is superhydrophobic ($36 \text{ mm} \times 36 \text{ mm} \times 3 \text{ mm}$), while the top plate is a normal copper plate ($76 \text{ mm} \times 76 \text{ mm} \times 3.5 \text{ mm}$). Acrylic blocks are used as stands to support the copper plates. A high voltage (HV) DC power supply from Spellman is used in the experiment. The positive electrode is connected to the bottom plate, while the top plate is grounded as shown in Figs. 5 and 6. The gap widths are set at 5 mm, 6 mm, 7 mm and 8 mm. It should be noted that the maximum voltage that can be provided by the equipment is 6 kV.

A syringe with a Terumo needle is used to create 2-mm-diameter droplets. The high-speed camera used is Phantom ir300, with a maximum resolution of 800×600 pixels at the frame rate of 6688 frames per second. To record the jumping droplets, a Nikon 105 mm F/2.8 Micro-Nikkor lens is mounted on the high-speed camera. The frame rate used during the test is 800 frames per second. Light bulbs are required to compensate for the insufficient light. In order to determine the electrical voltage threshold, the HV power supply is adjusted at 500-V increments until the droplet starts departing from the superhydrophobic surface. Next, the

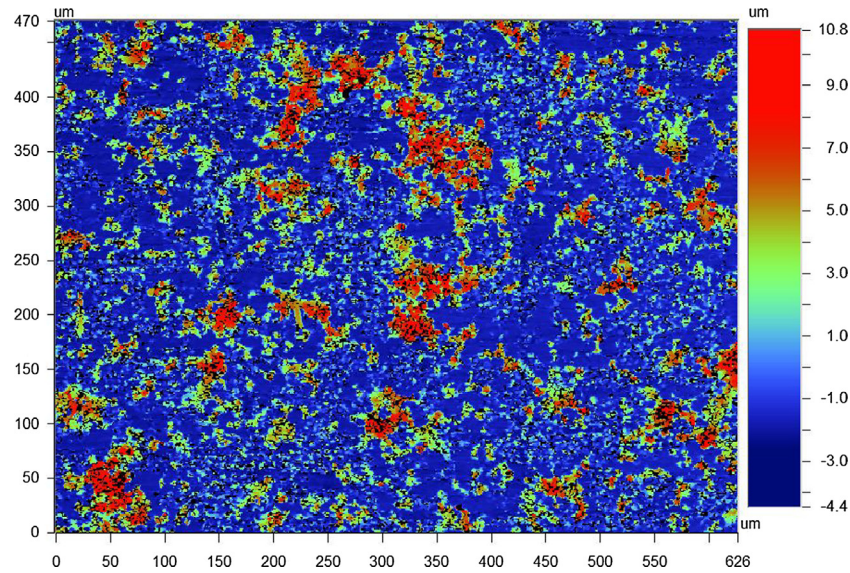


Fig. 4. The surface roughness of the superhydrophobic surface, the scale on x-axis and y-axis showing the measured area on the superhydrophobic surface, and the legend bar showing the surface roughness scale.

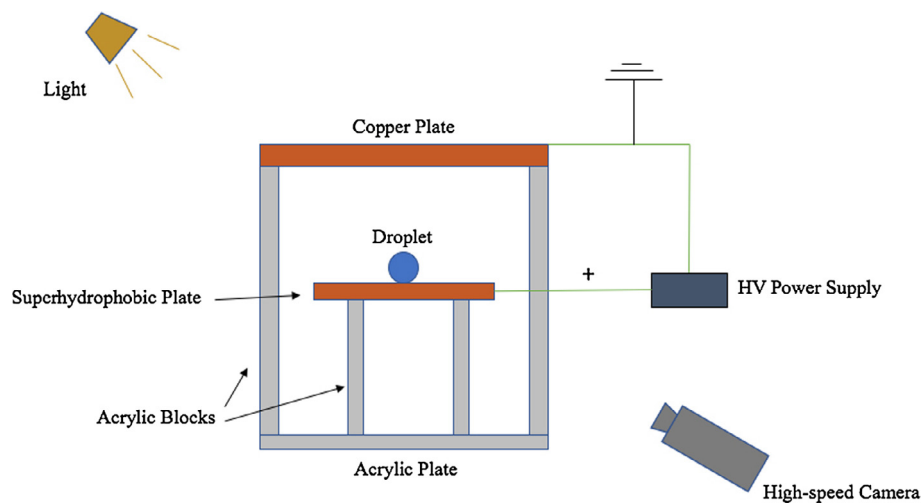


Fig. 5. A schematic diagram of the experimental setup of the jumping droplet under the electric fields.

test is conducted with a 100-V decrease until the voltage threshold is determined. This step is repeated 5 times. With the electrical voltage threshold for each gap width, the experiment is also repeated 5 times to determine the average droplet velocity and the travelling time of the droplets.

4. Results and discussions

4.1. Study of the electrical voltage threshold and the electric field threshold

Table 1 shows the results of the electrical voltage threshold and the electric field threshold required to lift droplets at different gap widths. It should be noted that the electric field threshold shown in Table 1 is calculated based on the voltage threshold and the gap width. It can be seen that the voltage threshold varies between 3.3 kV and 6 kV within the gap width from 5 mm to 8 mm. In detail, when the gap width is increased by 1 mm, the voltage threshold consistently increases by 0.9 kV, implying a linear rela-

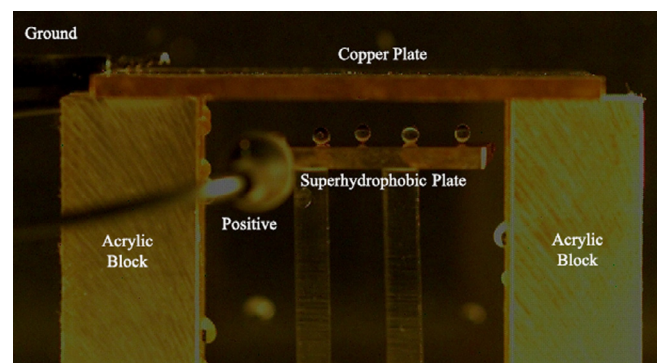


Fig. 6. The experimental setup of the jumping droplets under electric fields.

tionship between the gap width and the electrical voltage threshold as shown in Fig. 7. On the other hand, the electric field threshold non-linearly increases with an increase in the gap width.

Table 1

The electrical voltage threshold and the electric field threshold required to lift the droplet at different gap widths.

Gap width (mm)	Voltage threshold (kV)	Electric field threshold (V/mm)
5	3.3	660
6	4.2	700
7	5.1	729
8	6.0	750

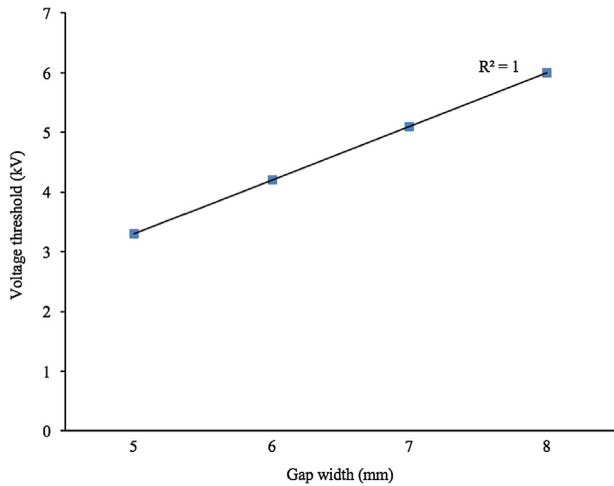


Fig. 7. Voltage threshold at each gap width.

From a 5-mm gap width to a 6-mm gap width, the electric field threshold increases by 40 V/mm, while an increment of 21.43 V/mm is observed with a 1-mm increase in the gap width from 7 mm to 8 mm. Thus, the electric field increment declines as the gap widens. If the trend in Fig. 7 continues, the maximum electric field will reach 900 V/mm. However, it should be noted that the non-linear increase between the electric field threshold and the

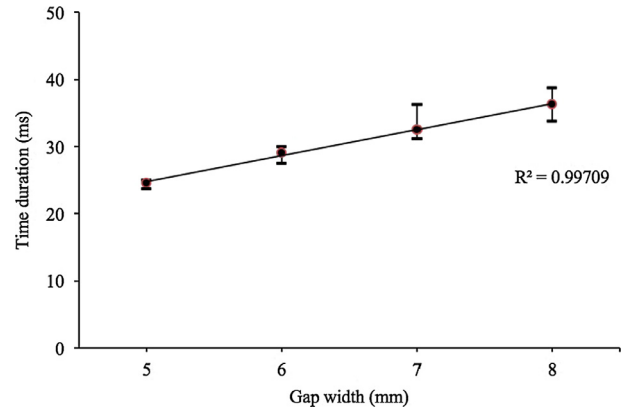


Fig. 9. Jumping duration of jumping droplets at each gap width.

gap width may be due to the fringing electric fields at the edges of the parallel plates [42].

4.2. Study of the jumping duration and the jumping velocity

In this section, the effects of the electrical voltage threshold on jumping duration and jumping velocity are discussed. The experiments are recorded by a high-speed camera, and the video is cut into many single frames. Frames at the time the droplet departs from the bottom plate to the top plate are counted and divided by the frame rate. It is found that the droplets constantly change their positions in the parallel electric field, implying that there is constant velocity. Fig. 8 shows the jumping droplet motion at the gap widths of 7 mm and 8 mm. In the first frame (left-most frame), when the electrical charge is approaching its threshold value, the droplet is slightly elongated and starts to form an elliptical shape, showing a tendency to depart from the surface even though the bottom of the droplet is pinned down to the surface. However, in mid-air, the shape of the droplet remains spherical. Fig. 9 shows the results of travelling duration of jumping droplets due to the

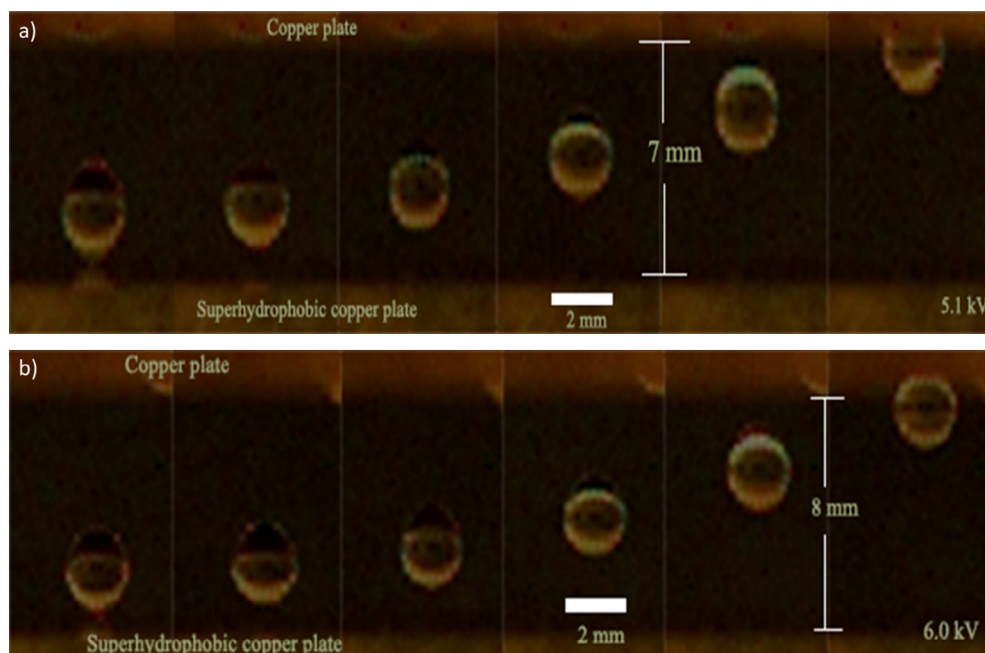


Fig. 8. A jumping droplet on the superhydrophobic surface with each frame showing the position of the jumping droplet under (a) 5.1 kV electrical voltage and 7 mm gap width, (b) 6.0 kV electrical voltage and 8 mm gap width.

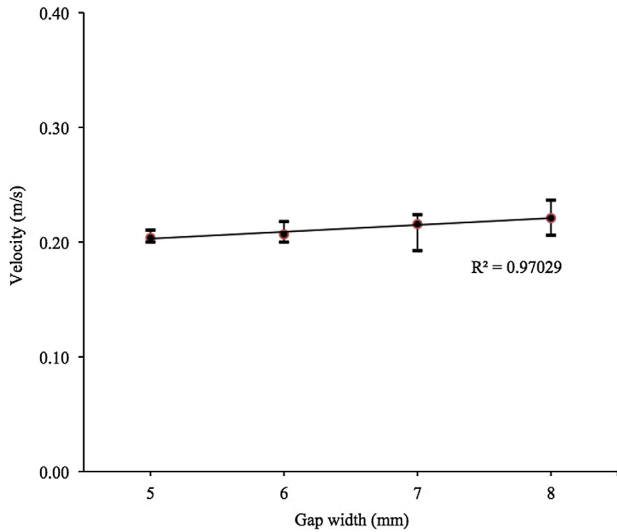


Fig. 10. Jumping droplet velocity at each gap width.

electrical voltage threshold at different gap widths. It is found that when the gap width increases, the jumping droplets take longer to complete the journey. Fig. 10 shows the results of jumping droplet velocity at different gap widths. From Fig. 10, it can be observed that an almost constant velocity of the jumping droplets is obtained at different gap widths (i.e. it should be noted that the velocity of jumping droplets is calculated from the gap width and the travelling time recorded by the high-speed camera). This means that the drag force due to the air resistance as well as the gravitational force due to the droplet volume constantly acts on the droplets regardless of the gap width. The velocities of the droplets are then used to determine the jumping droplet charges, which is discussed in detail in the next section.

4.3. Study of droplet charges during flight

After the droplet velocity is determined, the droplet charge due to the electrical voltage threshold can be identified. A mathematical model is developed to determine the relationship among the electric field threshold, the gap width and the size of droplets. This model can be used to estimate the amount of charge required to move a macro-sized droplet from the bottom plate to the top plate. However, it should be noted that this model is only applicable to the applied vertical electric fields with gap widths from 5 mm to 8 mm.

The following assumptions are made for the model development

- (1) The jumping droplet is assumed to maintain its spherical geometry while jumping in the air, resulting in a constant droplet radius. This assumption is verified by the Weber number which is the ratio of the inertia stress causing the droplet deformation to the surface tension resisting the deformation.

$$We = \frac{\rho_a v_d^2 (2r_0)}{\gamma}, \quad (3)$$

where γ and ρ_a represent the surface tension of water and air density, respectively, v_d denotes the droplet velocity, and r_0 is the radius of droplet. After substituting all parameters, the Weber number can be estimated. It is found that the Weber numbers at all different conditions are less than 0.002, implying that the fluid particle can be assumed to be a spherical shape [43].

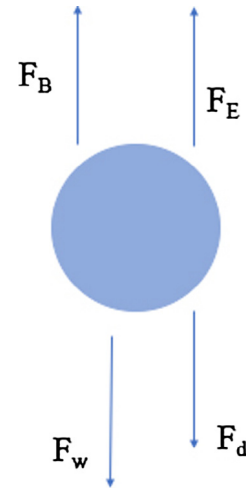


Fig. 11. The free body diagram of a moving droplet under a vertical electric field.

- (2) The jumping droplet velocity is assumed to be constant resulting in zero inertia force.
- (3) The permittivities and the electric conductivities of water and air are uniform.
- (4) No horizontal force exerts on the droplets in mid-air.

In order to determine the electrical charge, four vertical forces exerting on a droplet in mid-air are analyzed. The resistance force consists of the drag force ($F_D = \frac{1}{2} C_D \rho_a v_d^2 A$) and the gravitational force ($F_w = \frac{4}{3} \pi r_0^3 g \rho_w$), while the moving forces are the buoyancy force ($F_B = \rho_a g V_d$) and the electrostatic force or the coulomb force ($F_E = QE = Q \frac{V}{L}$). Fig. 11 shows the free body diagram of all the above-mentioned forces exerting on a droplet while it is moving from the bottom plate to the top one.

Due to the fact that the density of water is much larger than that of air ($\rho_w \gg \rho_a$), the buoyancy force can be neglected. Thus, the electrical charge can be determined after balancing all the forces, and it is expressed as

$$Q = \left[\frac{4}{3} \pi r_0^3 g \rho_w + \frac{1}{2} C_D \rho_a v_d^2 \pi r_0^2 \right] \frac{L}{V}, \quad (4)$$

where L , V , v_d and Q represent the gap width, the electrical voltage, the droplet velocity and the droplet charge, respectively. It should be noted that the average radius of the droplet (r_0) is 1×10^{-3} m, the water density (ρ_w) at 20 °C is 997 kg/m³, the gravitational acceleration (g) at sea level is 9.81 m/s² and the air density (ρ_a) at 20 °C is 1.184 kg/m³. The drag coefficient (C_D), as a function of Reynold number ($Re = \frac{\rho_a v_d (2r_0)}{\mu}$), is obtained from Eq. (5) [44].

$$C_D = \frac{24}{Re} + \frac{2.6 \left(\frac{Re}{5} \right)}{1 + \left(\frac{Re}{5} \right)^{1.52}} + \frac{0.411 \left(\frac{Re}{263000} \right)^{-7.94}}{1 + \left(\frac{Re}{263000} \right)^{-8}} + \left(\frac{Re^{0.8}}{461000} \right). \quad (5)$$

Given the velocities of the jumping droplets obtained from the experiment, the droplet charges at each gap width can be determined using Eq. (4). Table 2 illustrates the calculated average droplet charge per droplet surface area at different gap widths. The results show that although the electric field threshold increases with the gap width, the average droplet charge shows the opposite result. In other words, the droplet charge decreases with an increase in the electric field threshold. Moreover, it is mentioned in the previous section that due to the trend in Fig. 7, the electric field threshold will reach 900 V/mm. This means that although the droplet charge is inversely proportional to the electric field threshold as shown in Eq. (4), the droplet charge does not tend

Table 2
The average charge of droplets at different gap widths.

Gap width (mm)	Average charge ($\mu\text{C}/\text{m}^2$)	Electrostatic force (μN)
5	4.96	41.2
6	4.68	41.2
7	4.50	41.2
8	4.37	41.2

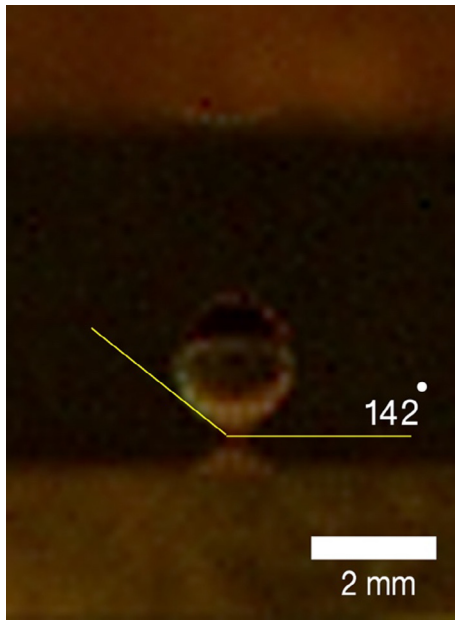


Fig. 12. The critical contact angle of the elongated droplet before lift-off.

to reach zero, but approaches a certain value at the electric field threshold of 900 V/mm. It should be noted that this inverse relationship has never been reported in previous studies on the moving macro-sized water droplet in the vertical electric field. In addition, the results in Table 2 show a constant electrostatic force acting on the jumping droplet, regardless of the electric field threshold and the gap width. That means the electrostatic force of the jumping droplet in mid-air is independent of the gap width and its electric field threshold.

4.4. Study of the lift-off mechanism and charging relaxation time

Although the electrostatic force acting on the droplet during the flight is found to be constant as mentioned in the previous section, determining the electrostatic force and the adhesion force of the droplet at the substrate of the electrode can provide more insight into the lift-off mechanism. As shown in Fig. 12, the critical contact angle of the elongated droplet from the experiment with the applied electric field threshold is approximately 142° regardless of the gap width. This value is close to the receding contact angle of 141.45° of the water droplet shown in Fig. 3, which is in line with the conclusion drawn by Gliere et al. [32] stating that the contact line collapses when the contact angle reaches either the receding angle or 90° .

By using Eq. (1), the maximum electrostatic force acting on the droplet before lift-off and the maximum adhesion force between the substrate and the droplet are $154.2 \mu\text{N}$ and $113.2 \mu\text{N}$, respectively. These forces are constant regardless of the gap width and its electric field threshold. Thus, it means that the maximum electrostatic force occurring on the surface of the electrode is independent of the gap width and its electric field. This result is in line with

the findings reported in the previous section. However, when the constant maximum electrostatic force of the droplet on the electrode is compared with the constant electrostatic force in mid-air, it is shown that the electrostatic force acting on the jumping droplet in mid-air accounts for 27% of the maximum electrostatic force acting on the droplet on the electrode before lift-off. It should be highlighted that this result has never been reported in any prior studies.

Moreover, in the current study, the droplet is experimentally studied in air with the uniform permittivity (ϵ) and electric conductivity (σ) of 8.85×10^{-12} F/m [34] and 0.9×10^{-14} S/m [45], respectively. By using Eq. (2), the relaxation time of the air as the medium fluid is approximately 983 s. As shown in Fig. 9, the time duration of the jumping droplet between two electrodes is less than 40 ms. Thus, the decay of the droplet charge in the current study can be negligible. The droplet velocity is constant, resulting in a constant drag force. This constant velocity is also observed in the experiment as mentioned in the previous section. Additionally, due to the same droplet volume, the gravitational force is also constant resulting in a constant electrostatic force regardless of the gap width or the applied electric field. This shows that the electrostatic force and the velocity of the droplet tends to remain constant in the electrostatic-induced jumping in a low conductivity medium fluid. According to the results reported in previous sections, when the gap width increases, the electrical voltage threshold and the electric field threshold also increase. Thus, in order for the electrostatic force acting on the droplet to remain constant, the charge must decrease with an increase in the gap width.

5. Comparing findings with other studies

5.1. The voltage threshold and the electric field threshold

As shown in Table 3, the experimental conditions of the current study are different compared to those of the previous studies in terms of the medium fluid used, the gap width and the droplet size. It should be noted that to the researchers' knowledge to date, the current study is the only study on the electrostatic-induced macro-sized droplet that attempts to vary the gap width. In the previous study by Takeda et al. [19], a 9-kV voltage was applied to two parallel plates with the gap width of 10 mm to induce the jumping phenomenon of a 2-mm-diameter droplet. However, they did not mention whether the preset voltage was the threshold value or not. In the experiment conducted by Roux et al. [20], NaCl solution droplets were experimented in a light-mineral-oil condenser. The results showed that the electric field threshold increased with the droplet size. With the gap width of 33 mm, the electric field threshold ranged from 110 V/mm to 175 V/mm resulting in the electrical voltage thresholds of 3.63 kV and 5.78 kV, respectively. In the investigation of the droplet dynamics performed by Khayari et al. [21], a water droplet was placed in corn oil. The voltage threshold and the electric field threshold used to initiate the jumping phenomenon of a 2.674-mm diameter droplet at the fixed gap width of 20 mm were 3.4 kV and 170 V/mm, respectively. Although the voltage thresholds of the current study, of the study by Roux et al. [20] and of the study by Khayari et al. [21] are similar in terms of magnitude, the gap widths in the current study are much smaller than those in the other two studies. As a result, the large difference in the electric field threshold between the current study and the previous studies can be observed. One reason is that light mineral oil and corn oil were used as the medium fluids. As shown in Table 4, the density of these two types of oil is approximately 700 times greater than that of air. Thus, the buoyancy force and the electrostatic force become two major driving forces in these previous studies [20,21]. On the other hand, the

Table 3
Threshold comparison with previous similar studies.

	Droplet type (–)	Droplet radius (mm)	Medium fluid (–)	Gap width (mm)	Electric field direction (–)	E-Field threshold (V/mm)	Voltage threshold (kV)
Current study	Water	1	Air	5–8	Vertical	660–750	3.3–6.0
Roux et al. [20]	NaCl	0.5–0.78	Light mineral oil	33	Vertical	110–175	3.6–5.8
Khayari et al. [21]	Water	1.337	Corn oil	20	Vertical	170	3.4
Takeda et al. [19]	Water	1	Air	10	Vertical	N/A	N/A
Jung et al. [23]	Water	0.363–0.726	Silicon oil	10	Horizontal	N/A	N/A
Jalaal et al. [24]	Water	0.15–1.75	Transformer oil	38	Horizontal	N/A	N/A

Table 4
Relaxation time comparison with previous similar studies.

	Medium fluid	Density (kg/m ³)	Permittivity $\times 10^{-12}$ (F/m)	Conductivity $\times 10^{-12}$ (S/m)	Relaxation time (s)
Current study	Air	1.23	8.85	0.009	983.33
Roux et al. [20]	Light mineral oil	840	18.67	0.4	46.8
Khayari et al. [21]	Corn oil	916	26.9	19.0	1.42
Takeda et al. [19]	Air	1.23	8.85	0.009	983.33
Jung et al. [23]	Silicon oil	957.24	24.35	0.1	243.50
Jalaal et al. [24]	Transformer oil	841.9	18.67	3.3	5.66

electrostatic force is the sole pushing force in the current study because the buoyancy force is neglected due to the very low density of air compared to that of water.

However, it should be noted that the study by Khayari and Perez [22] did not involve any liquid droplets on the electrode, but a plastic sphere covered by aluminum sheets and aluminum spheres. Aluminum has its own electrical conductivity which is much greater than that of water. Also, the radii of these three spheres were 2–5 times greater than that of the current study. Thus, the results of the study by Khayari and Perez [22] and of the current study cannot be compared.

5.2. Droplet charges and forces

For the force analysis of the jumping droplets, although all studies including the present one have similar approaches, some major and minor differences in the findings have been observed. In Roux et al.'s [20] and Khayari et al.'s studies [21], Maxwell's charge of the droplet on the electrode was applied. This leads to the direct proportion between the electric field and the droplet charge. In other words, the droplet charge increases with an increase in the electric field. However, it should be noted that Maxwell's charge can be used if and only if the droplet size is negligible compared to the gap width. While the ratios of the gap width to the droplet radius of the two prior studies [20,21] are 66 and 15, respectively, such ratio of the current research is only 8. This means that the droplet size in the current study cannot be neglected compared to the gap width. Thus, Maxwell's charge in the current study is considered invalid. However, the droplet charge can still be obtained from the force balance equation in mid-air. Moreover, it should be noted that in the study of Roux et al. [20] and Khayari et al. [21], the force analysis was solely performed with droplets on the electrode, while the current study has analyzed the electrostatic force both on the electrode before lift-off and in mid-air.

5.3. The lift-off mechanism and charge relaxation time

Apart from the electric field threshold, the droplet charge and the force analysis, the lift-off mechanism is also important. The discussions regarding such a phenomenon can be found in Khayari et al. [21], Gliere et al. [32] and the present study. A droplet on the lower electrode elongates due to the electrostatic force. After the contact angle reaches 90° or its receding angle, the contact line

collapses, and the droplet starts jumping. The maximum adhesion force and the maximum electrostatic force are also found in the present study.

Moreover, as shown in Table 4, due to the very high electric conductivity of the medium fluid reported in Khayari et al.'s study [21], the relaxation time observed in the study was only 1.42 s. This means that the droplet charge decays, and the droplets do not reach the top plate and fall to the lower electrode due to the gravitational force. As a result, the droplet velocity of the study [21] is not constant, resulting in the non-constant electrostatic force acting on a droplet in the medium fluid. However, the electric conductivity of the current study is very low, leading to the relaxation time of 983 s. The experimental results also show that the maximum time duration of the jumping droplet is less than 40 ms. This means that the decay of the charge in the current study is negligible. As a result, the droplet velocity and the electrostatic force in each gap width in the present study are also constant throughout the flight.

6. Conclusion

In this study, airborne jumping water droplets on a superhydrophobic surface with various gap widths and electric fields are experimentally studied. The electrical voltage threshold, the electric field threshold and the droplet charge required to lift droplets at different gap widths are determined. It is found that the electrical voltage threshold and the electric field threshold increase with the gap width. A linear relationship is found between the electrical voltage threshold and the gap width, while the electric field threshold is in a non-linear relationship with the gap width. This may be caused by the fringing electric field at the edges of the parallel plates. In addition, the droplet charge is found to be inversely proportional to the electric field threshold. Moreover, the electrostatic force acting on the droplet in mid-air is constant, is independent to the gap width and the electric field threshold, and accounts for 27% of the maximum electrostatic force acting on the droplet on the electrode surface. Additionally, the lift-off mechanism and the relaxation time obtained from the current study is in line with those of the previous research studies. The outcome of this study provides insights into the electrostatic-induced droplet dynamics and minimum energy required to remove macro-sized droplets from the superhydrophobic surface which can minimize progres-

sive flooding, leading to enhanced condensation heat transfer performance.

Acknowledgments

The funding sources for this research are provided by the Hong Kong Research Grant Council via General Research Fund (GRF) account 16202517 and Collaborative Research Fund (CRF) account C6022-16G, and by The Hong Kong University of Science and Technology (HKUST) Initiation Grant (accounts IGN16EG05).

Conflict of interest

Disclosure statement: We declare that we do not have any actual or potential conflict of interest including any financial, personal or other relationships with other people or organizations within three years of beginning the work submitted that could inappropriately influence (bias) our work.

References

- [1] T.B. Peters, M. McCarthy, J. Allison, F.A. Dominguez-Espinosa, D. Jenicke, H.A. Kariya, W.L. Staats, J.G. Brisson, J.H. Lang, E.N. Wang, Design of an integrated loop heat pipe air-cooled heat exchanger for high performance electronics, *IEEE Trans. Comp. Packag. Manuf. Technol.* 2 (2012) 1637–1648, <http://dx.doi.org/10.1109/TCPMT.2012.2207902>.
- [2] R.N. Leach, F. Stevens, S.C. Langford, J.T. Dickinson, Dropwise condensation: experiments and simulations of nucleation and growth of water drops in a cooling system, *Langmuir* 22 (2006) 8864–8872, <http://dx.doi.org/10.1021/la061901+>.
- [3] J.M. Beer, High efficiency electric power generation: the environmental role, *Prog. Energy Combust. Sci.* 33 (2007) 107–134, <http://dx.doi.org/10.1016/j.pecs.2006.08.002>.
- [4] M.A.K. Azad, W. Barthlott, K. Koch, Hierarchical surface architecture of plants as an inspiration for biomimetic fog collectors, *Langmuir* 31 (2015) 13172–13179, <http://dx.doi.org/10.1021/acs.langmuir.5b02430>.
- [5] S. Kim, K.J. Kim, Dropwise condensation modeling suitable for superhydrophobic surfaces, *J. Heat Transfer* 133 (2011) 81502, <http://dx.doi.org/10.1115/1.4003742>.
- [6] N. Miljkovic, E.N. Wang, Condensation heat transfer on superhydrophobic surfaces, *MRS Bull.* 38 (2013) 397–406, <http://dx.doi.org/10.1557/mrs.2013.103>.
- [7] J.W. Rose, Dropwise condensation theory and experiment: a review, *J. Power Energy, Part A* 216 (2002) 115–128, <http://dx.doi.org/10.1243/09576500260049034>.
- [8] J.B. Boreyko, C.H. Chen, Self-propelled dropwise condensate on superhydrophobic surfaces, *Phys. Rev. Lett.* 103 (2009) 184501, <http://dx.doi.org/10.1103/PhysRevLett.103.184501>.
- [9] Y. Nam, H. Kim, S. Shin, Energy and hydrodynamic analyses of coalescence-induced jumping droplets, *Appl. Phys. Lett.* 103 (2013) 161601, <http://dx.doi.org/10.1063/1.4825273>.
- [10] X. Liu, P. Cheng, X. Quan, Lattice Boltzmann simulations for self-propelled jumping of droplets after coalescence on a superhydrophobic surface, *Int. J. Heat Mass Transf.* 73 (2014) 195–200, <http://dx.doi.org/10.1016/j.ijheatmasstransfer.2014.01.060>.
- [11] F. Liu, G. Ghigliotti, J.J. Feng, C.H. Chen, Numerical simulations of self-propelled jumping upon drop coalescence on nonwetting surfaces, *J. Fluid Mech.* 752 (2014) 39–65, <http://dx.doi.org/10.1017/jfm.2014.320>.
- [12] R. Enright, N. Miljkovic, J. Sprittles, K. Nolan, R. Mitchell, E.N. Wang, How coalescing droplets jump, *ACS Nano* 8 (2014) 10352–10362, <http://dx.doi.org/10.1021/nn503643m>.
- [13] K. Rykaczewski, A.T. Paxson, S. Anand, X. Chen, Z. Wang, K.K. Varanasi, Multimode multidrop serial coalescence effects during condensation on hierarchical superhydrophobic surfaces, *Langmuir* 29 (2013) 881–891, <http://dx.doi.org/10.1021/la304264g>.
- [14] X. Chen, J.A. Weibel, S.V. Garimella, Exploiting microscale roughness on hierarchical superhydrophobic copper surfaces for enhanced dropwise condensation, *Adv. Mater. Interfaces* 2 (2015) 1400480, <http://dx.doi.org/10.1002/admi.201400480>.
- [15] N. Miljkovic, R. Enright, Y. Nam, K. Lopez, N. Dou, J. Sack, E.N. Wang, Jumping-droplet-enhanced condensation on scalable superhydrophobic nanostructured surfaces, *Nano Lett.* 13 (2012) 179–187, <http://dx.doi.org/10.1021/nl303835d>.
- [16] C. Graham, P. Griffith, Drop size distributions and heat transfer in dropwise condensation, *Int. J. Heat Mass Transfer* 16 (1973) 337–346, [http://dx.doi.org/10.1016/0017-9310\(73\)90062-8](http://dx.doi.org/10.1016/0017-9310(73)90062-8).
- [17] P. Birbarah, Z. Li, A. Pauls, N. Miljkovic, A comprehensive model of electric-field-enhanced jumping-droplet condensation on superhydrophobic surfaces, *Langmuir* 31 (2015) 7885–7896, <http://dx.doi.org/10.1021/acs.langmuir.5b01762>.
- [18] N. Miljkovic, D.J. Preston, R. Enright, E.N. Wang, Electric-field-enhanced condensation on superhydrophobic nanostructured surfaces, *ACS Nano* 7 (2013) 11043–11054, <http://dx.doi.org/10.1021/nn404707j>.
- [19] K. Takeda, A. Nakajima, K. Hashimoto, T. Watanabe, Jump of water droplet from a super-hydrophobic film by vertical electric field, *Surf. Sci.* 519 (2002) L589–L592, [http://dx.doi.org/10.1016/S0039-6028\(02\)02144-1](http://dx.doi.org/10.1016/S0039-6028(02)02144-1).
- [20] J.M. Roux, J.L. Achard, Y. Fouillet, Forces and charges on an undeformable droplet in the DC field of a plate condenser, *J. Electrostat.* 66 (2008) 283–293, <http://dx.doi.org/10.1016/j.elstat.2008.01.008>.
- [21] A. Khayari, A.T. Perez, F.J. Garcia, A. Castellanos, Dynamics and deformation of a drop in a DC electric field, *Conference on Electrical Insulation and Dielectric Phenomena*, Albuquerque, 2003, <http://dx.doi.org/10.1109/CEIDP.2003.1254946>.
- [22] A. Khayari, A.T. Perez, Charge acquired by a spherical ball bouncing on an electrode: comparison between theory and experiment, *IEEE Trans. Dielectr. Electr. Insulat.* 9 (2002) 589–595, <http://dx.doi.org/10.1109/TDEI.2002.1024437>.
- [23] Y.M. Jung, H.C. Oh, I.S. Kang, Electrical charging of a conducting water droplet in a dielectric fluid on the electrode surface, *J. Colloid Interface Sci.* 322 (2008) 617–623, <http://dx.doi.org/10.1016/j.jcis.2008.04.019>.
- [24] M. Jalaal, B. Khorshidi, E. Esmailzadeh, An experimental study on the motion, deformation and electrical charging of water drops falling in oil in the presence of high voltage D.C. electric field, *Exp. Therm. Fluid Sci.* 34 (2010) 1498–1506, <http://dx.doi.org/10.1016/j.expthermflusci.2010.07.014>.
- [25] K.M. Wisdom, J.A. Watson, X. Qu, F. Liu, G.S. Watson, C.H. Chen, Self-cleaning of superhydrophobic surfaces by self-propelled jumping condensate, *Proc. Natl. Acad. Sci. United States of America* 110 (2013) 7992–7997, <http://dx.doi.org/10.1073/pnas.1210770110>.
- [26] J.B. Boreyko, C.-H. Chen, Vapor chambers with jumping-drop liquid return from superhydrophobic condensers, *Int. J. Heat Mass Transfer* 61 (2013) 409–418, <http://dx.doi.org/10.1016/j.ijheatmasstransfer.2013.01.077>.
- [27] J.B. Boreyko, Y. Zhao, C.H. Chen, Planar jumping-drop thermal diodes, *Appl. Phys. Lett.* 99 (2011) 234105, <http://dx.doi.org/10.1063/1.3666818>.
- [28] S. Jung, M.K. Tiwari, N.V. Doan, D. Poulikakos, Mechanism of supercooled droplet freezing on surfaces, *Nat. Commun.* 3 (2012) 615, <http://dx.doi.org/10.1038/ncomms1630>.
- [29] J. Cheng, A. Vandadi, C.L. Chen, Condensation heat transfer on two-tier superhydrophobic surfaces, *Appl. Phys. Lett.* 101 (2012) 131909, <http://dx.doi.org/10.1063/1.4756800>.
- [30] A.Y.H. Cho, Contact charging of micron-sized particles in intense electric fields, *J. Appl. Phys.* 35 (1964) 2561–2564, <http://dx.doi.org/10.1063/1.1713799>.
- [31] N. Lebedev, I. Skal'skaya, Force acting on a conducting sphere in field of a parallel plate condenser, *Sov. Phys. Tech. Phys.* 7 (1962) 268–270.
- [32] A. Gliere, J.M. Roux, J.L. Achard, Lift-off of a condensing sessile drop in an electric field, *Microfluidics Nanofluidics* 15 (2013) 207–218, <http://dx.doi.org/10.1007/s10404-013-1144-6>.
- [33] H.A. Haus, J.R. Melcher, *Electromagnetic Fields and Energy*, Prentice Hall, New Jersey, 1989.
- [34] U.S. Inan, A.S. Inan, *Engineering Electromagnetics*, Addison-Wesley, Calif, 1989.
- [35] T. Onda, S. Shibuchi, N. Satoh, K. Tsujii, Super-water-repellent fractal surfaces, *Langmuir* 12 (1996) 2125–2127, <http://dx.doi.org/10.1021/la950418o>.
- [36] Y. Wu, H. Sugimura, Y. Inoue, O. Takai, Thin films with nanotextures for transparent and ultra water-repellent coatings produced from trimethylmethoxysilane by microwave plasma CVD, *Chem. Vap. Deposition* 8 (2002) 47–50.
- [37] K. Tadanaga, J. Morinaga, A. Matsuda, T. Minami, Superhydrophobic-superhydrophilic micropatterning on flowerlike alumina coating film by the sol-gel method, *Chem. Mater.* 12 (2000) 590–592, <http://dx.doi.org/10.1021/cm990643h>.
- [38] Z. Sun, X. Chen, H. Qiu, Experimental investigation of a novel asymmetric heat spreader with nanostructure surfaces, *Exp. Therm. Fluid Sci.* 52 (2014) 197–204, <http://dx.doi.org/10.1016/j.expthermflusci.2013.09.011>.
- [39] I.A. Larmour, S.E. Bell, G.C. Saunders, Remarkably simple fabrication of superhydrophobic surfaces using electroless galvanic deposition, *Angew. Chem.* 119 (2007) 1740–1742, <http://dx.doi.org/10.1002/ange.200604596>.
- [40] Silver nitrate ACS reagent $\geq 99\%$ (CAS Number 7761-88-8), Sigma-Aldrich, Retrieved from <<http://www.sigmaaldrich.com/catalog/product/sigald/209139>>.
- [41] Heptadecafluoro-1-decanethiol $\geq 96\%$ (CAS Number 34143-74-3), Sigma Aldrich, Retrieved from <<http://www.sigmaaldrich.com/catalog/product/aldrich/08686>>.
- [42] M.C. Hegg, A.V. Mamishev, Influence of variable plate separation on fringing electric fields in parallel-plate capacitors, in: *The 2004 IEEE International Symposium on Electrical Insulation*, Indianapolis, 2004, <http://dx.doi.org/10.1109/ELINSL.2004.1380606>.
- [43] E. Loth, Quasi-steady shape and drag of deformable bubbles and drops, *Int. J. Multiph. Flow* 34 (2008) 523–546, <http://dx.doi.org/10.1016/j.ijmultiphaseflow.2007.08.010>.
- [44] F.A. Morrison, *An Introduction to Fluid Mechanics*, Cambridge University Press, New York, 2013.
- [45] S.D. Pawar, P. Murugavel, D.M. Lal, Effect of relative humidity and sea level pressure on electrical conductivity of air over Indian Ocean, *J. Geophys. Res.* 144 (2009) D02205, <http://dx.doi.org/10.1029/2007JD009716>.